Research Paper

PAIN®

Cell type–specific super-resolution imaging reveals an increase in calcium-permeable AMPA receptors at spinal peptidergic terminals as an anatomical correlate of inflammatory pain

Stephen G. Woodhams[a,*], Robert Markus[b], Peter R.W. Gowler[a], Timothy J. Self[b], Victoria Chapman[a]

Abstract

Spinal hyperexcitability is a key event in the development of persistent pain, and arises partly from alterations in the number and localization of α-amino-3-hydroxy-5-methyl-4-isoxazole propionate (AMPA)-type glutamate receptors. However, determining precisely where these changes occur is challenging due to the requirement for multiplex labelling and nanoscale resolution. The recent development of super-resolution light microscopy provides new tools to address these challenges. Here, we apply combined confocal/direct STochastic Optical Reconstruction Microscopy (dSTORM) to reveal changes in calcium-permeable subunits of AMPA-type glutamate receptors (GluA1) at identified spinal cord dorsal horn (SCDH) peptidergic axon terminals in a model of inflammatory pain. L4/5 lumbar spinal cord was collected from adult male C57BL/6J mice 24 hours after unilateral hind paw injection of saline or 1% carrageenan (n = 6/group). Tissue was immunolabelled for markers of peptidergic axon terminals (substance P; SP), presynaptic active zones (Bassoon), and GluA1. Direct stochastic optical reconstruction microscopy revealed a 59% increase in total GluA1 immunolabelling in the SCDH in the carrageenan group, which was not detected by confocal microscopy. Cell type–specific analyses identified a 10-fold increase in GluA1 localized to SP^+ structures, and identified GluA1 nanodomains that scaled with behavioural hypersensitivity, and were associated with synaptic release sites. These findings demonstrate that dSTORM has the sensitivity and power to detect nanoscale anatomical changes in the SCDH, and provides new evidence for synaptic insertion of $GluA1^+$-AMPA-Rs at spinal peptidergic nociceptive terminals in a model of inflammatory pain.

Keywords: Spinal sensitization, Inflammatory pain, Super-resolution imaging, AMPA-Rs, dSTORM

1. Introduction

The spinal cord dorsal horn (SCDH) is a key site in pain processing, receiving and integrating ascending input from the peripheral nervous system and descending modulatory input from the brain. The mammalian SCDH circuitry is highly complex, delineated into functionally distinct laminae,[37] each incorporating numerous diverse cell types with differing functions in somatosensation.[27] Determining precisely where and how alterations in the connectivity and excitability of this circuitry occur is a key requirement to elucidate the mechanisms underlying the development and maintenance of persistent pain states, and ultimately to identify much-needed novel analgesic strategies.

Significant recent advances have been made through the careful anatomical characterization of spinal excitatory[18] and inhibitory[6] interneurons via expression of neurochemical markers, and the use of single-cell RNA sequencing to delineate further subpopulations of both primary afferent fibers[44] and intrinsic SCDH neurons.[21] Long-term spinal synaptic plasticity has been demonstrated at the level of the population[15] and single cell[43,49] via electrophysiological recordings, and insights into the functional role of some of these populations have been provided via ablation,[10] chemogenetic silencing,[13] or optogenetic control.[20] However, to understand how each component contributes to the development and maintenance of spinal hypersensitivity in vivo requires quantification of alterations in synaptic physiology in a region- and cell type–specific manner in the intact circuitry.

Accumulation of calcium-permeable GluA1 subunits of α-amino-3-hydroxy-5-methyl-4-isoxazolepropionic acid glutamate receptors (AMPA-Rs) is required for calcium-dependent synaptic plasticity in many regions of the central nervous system.[39] GluA1 is expressed on numerous cell types in rodent spinal cord,[12,35] and spinal membrane expression of GluA1, but not GluA2, is elevated in the carrageenan model of inflammatory pain.[48] GluA1 is preferentially associated with the central terminals of peptidergic primary afferent fibers,[14,28] and functional evidence suggests a switch to calcium-mediated signaling

Sponsorships or competing interests that may be relevant to content are disclosed at the end of this article.

[a] Arthritis Research UK Pain Centre, School of Life Sciences, University of Nottingham, Medical School, Queen's Medical Centre, Nottingham, United Kingdom, [b] School of Life Sciences Imaging Centre (SLIM), School of Life Sciences, University of Nottingham, Medical School, Queen's Medical Centre, Nottingham, United Kingdom

**Corresponding author. Address: Arthritis Research UK Pain Centre, School of Life Sciences, University of Nottingham, Queen's Medical Centre, Nottingham NG7 2UH, United Kingdom. Tel.: +44(0)1158230154; fax: +44(0)1158230142. E-mail address: stephen.woodhams@nottingham.ac.uk (S.G.Woodhams).*

Supplemental digital content is available for this article. Direct URL citations appear in the printed text and are provided in the HTML and PDF versions of this article on the journal's Web site (www.painjournalonline.com).

PAIN 160 (2019) 2641–2650

http://dx.doi.org/10.1097/j.pain.0000000000001672

at these synapses in the complete Freund's adjuvant model of inflammation.[47] However, precisely where and how GluA1 expression changes remains unknown.

To date, characterizing the underlying anatomical correlates of plasticity has been restricted by the requirement for nanoscale resolution, multiplex labelling, and high-throughput analysis. Super-resolution imaging provides novel tools (reviewed in Refs. 24, 51) capable of revealing the anatomical correlates of altered neuronal function,[32] but these are yet to be applied to spinal cord tissue or studies of pain mechanisms. Herein, we use direct Stochastic Optical Reconstruction Microscopy (dSTORM)[38,52] to probe the spinal correlates of persistent synaptic plasticity and the contribution of spinal GluA1 in the carrageenan model of subacute inflammatory pain.

2. Methods

2.1. Animals

Studies were in accordance with U.K. Home Office Animals (Scientific Procedures) Act (1986) and ARRIVE guidelines.[26] Twelve adult male C57BL/6J mice were used for this study (Charles River, Margate, United Kingdom, 49-55 days at delivery). Mice were housed in groups of 3 in individually ventilated cages in a specific pathogen-free environment, with ad libitum access to standard mouse chow and water.

2.2. Carrageenan model

Mice were randomly assigned to receive a unilateral intraplantar administration of 10 μL 1% carrageenan or sterile saline (n = 6/group) into the right hind paw under brief isoflurane anaesthesia. Animals were monitored for 3 hours after recovery. Pain behaviour was assessed at baseline and 24 hours after injection by an experimenter blinded to treatment. Fifty percent paw withdrawal thresholds (PWTs) to von Frey filament stimulation were determined as previously described.[3] One saline-injected animal was excluded due to a misplaced injection.

2.3. Tissue processing

Mice were transcardially perfused under terminal anaesthesia (0.2 mL Euthatal, intraperitoneally [i.p.]) with sterile saline (50 mL, 0.9% NaCl), followed by fixation with 4% paraformaldehyde (PFA; 50 mL). The whole spinal column was removed and postfixed in 4% PFA for 48 hours. After extensive washing in 0.1M phosphate buffer (PB), the lumbar enlargement of the spinal cord was dissected out of the column, and tissue sections for combined confocal/STORM imaging prepared as previously described,[2] with some adaptations. Briefly, L4/5 lumbar spinal cord was embedded in 2% agarose, marked through the contralateral ventral gray matter with a 28 G needle, and 40 μm sections cut on a Leica V1000 vibratome.

2.4. Immunohistochemistry

Sections were triple labelled through free-floating immunohistochemistry for markers of peptidergic nociceptive terminals (substance P [SP][31,34]), presynaptic active zones (bassoon[9,42]), and GluA1$^+$-AMPARs[8,14] (see **Table 1** for antibody details). Sections were washed first in 0.1M PB, and then in 0.05M TRIS buffered saline (TBS). Nonspecific binding was blocked and tissue permeabilized through incubation with 1% bovine serum albumin (Sigma, Gillingham, United Kingdom), 0.3% Triton X100 (Sigma), in TBS (1 hour, RT). Sections were then incubated first with primary antibodies diluted in TBS (1 hour RT, 60 hours 4°C), followed by appropriate secondary antibodies (4 hours, dark, **Table 1**) after extensive washing. Finally, sections were mounted directly onto acetone-cleaned 18 × 18 mm coverslips and stored at 4°C in the dark until imaging. Negative control sections were incubated with TBS alone during primary incubations, followed by the same combination of secondary antibodies to enable determination of any nonspecific secondary binding.

2.5. Combined confocal/dSTORM

Immediately before imaging, sections were mounted onto a clean glass slide using a SecureSeal imaging spacer (Grace Labs, GBL654002, 9 mm × 0.12 mm) containing 9 μL abbelight smart kit (Abbelight, Paris, France). Images of the ipsilateral dorsal horn were collected on a Zeiss Elyra PS1 combined LSM780 and super-resolution imaging platform (Zeiss, Oberkochen, Germany) via α plan-apochromat 100×/1.46 objective lens (Zeiss) using 30° immersion oil and Zen Black imaging software.

Regions of interest (ROIs) with multiple SP$^+$/Bassoon$^+$ structures (presumed peptidergic nociceptive synapses) were selected from the medial superficial SCDH, <5 μm from the section surface. Confocal z stacks (*x* & *y*: 26.57 μm, z: 3 μm, pixel size 0.104 μm) were acquired (Supplementary Fig. 1A, available at http://links.lww.com/PAIN/A857) and the optimal optical section selected. Focus was maintained at this point using the automated Definite Focus system for dSTORM imaging (Supplementary Fig. 1B, available at http://links.lww.com/PAIN/A857). Fluorophores were bleached through step-wise increases of 150 mW 642 nm diode laser to 100% in TIRF-HP mode with camera gain set to 200 (Andor EM-CCD iXon Du 897, Belfast, Northern Ireland; pixel size 1.6 μm). 2D dSTORM images were then collected for 5000 25 ms cycles at 100% 642 nm power, with 2.5% 50 mW 405 nm diode laser in transfer mode to boost photoswitching (Supplementary Fig. 1C–E, available at http://links.lww.com/PAIN/A857). Three to four ROIs were imaged from at least one section per animal, and 4 animals per condition.

2.6. Image analysis

2.6.1. Confocal analysis

Single-plane, 3-channel confocal images were isolated from 3 μm z-stacks using FIJI and whole ROI mean gray intensity determined for each channel. Area of labelling was determined from binary images produced via Otsu auto-thresholding using the "analyse particles" function.

2.6.2. Stochastic optical reconstruction microscopy analysis

Localisation points (LPs) from dSTORM images were produced using the PALM module of Zeiss Zen Black with settings determined by preliminary experiments (see Supplementary Materials and Supplementary Fig. S2, available at http://links.lww.com/PAIN/A857). The total number of localisations within each field of view was then recorded and compared. For targeted cell type–specific analysis of SP$^+$ structures, combined confocal/STORM analysis was performed using the in-built functions in vividSTORM image analysis software[2] (freely available from https://sourceforge.net/projects/vividstorm/). SP$^+$ ROIs were manually selected from each confocal image using the free-form ROI drawing function. Bayesian cluster analysis[5] was used to identify individual filtered GluA1 clusters within each ROI using the in-built function within vividSTORM (see Supplementary Materials for

Table 1

Antibody details.

Primary antibody	Supplier/Cat. no.	Secondary antibody	Supplier/Catalogue no.
Rat anti-substance P,[31,34] 1:500	BIO-RAD, Hercules, CA (8450-0505)	Donkey anti-rat-AF488, 1:400	Invitrogen, Waltham, MA (A21208)
Mouse anti-bassoon,[9,42] 1:500	Abcam, Cambridge, United Kingdom (ab82958)	Goat anti-rabbit-CF568, 1:400	Stratech (Newmarket, United Kingdom) goat anti-rabbit IgG (111-005-003-JIR) + Sigma Mix-n-Stain CF568 labelling kit (MX568S50)
Rabbit anti-GluA1,[8,14] 1:250	Abcam (ab31232)	Donkey anti-mouse-AF647, 1:400	Invitrogen (A31571)

All antibodies have been previously validated. See Supplementary Materials (available at http://links.lww.com/PAIN/A857) for antibody specificity statement.

details, available at http://links.lww.com/PAIN/A857). Localization points from each cluster were then overlaid with confocal images, and visually assessed for association with a synapse. Clusters were classified as synapse-associated if overlapping with, or directly apposed to, confocal signal corresponding to a bassoon punctum, or non–synapse-associated if the closest LP was >20 nm distant from the nearest bassoon labelling, as assessed using the ruler tool in vividSTORM.

2.7. Statistical analyses

Data were analysed using Prism 7.0 software (GraphPad, La Jolla, CA) using Kruskal–Wallis, Mann–Whitney *U*, or Wilcoxon signed ranks tests as appropriate. Correlations were assessed using nonparametric Spearman test. Normality of data was assessed using D'Agostino–Pearson omnibus test, and because all data were nonparametric, they are reported as median ± interquartile range (IQR). $P < 0.05$ was considered statistically significant.

3. Results

3.1. Carrageenan induces a sustained inflammatory pain phenotype in mice

Intraplantar injection of saline produced no visible inflammation or change in ipsilateral PWTs at 24 hours (**Figs. 1A and B**). By contrast, injection of 1% carrageenan produced significant edema, visible within hours and still apparent after 24 hours (**Fig. 1A**, right), accompanied by a pronounced reduction in mechanically-evoked ipsilateral hind paw withdrawal thresholds compared with preinjection values (**Fig. 1B**; median change −55%, IQR 35%-80%, $P = 0.0156$).

3.2. Confocal analyses does not detect changes in spinal GluA1 expression after carrageenan

Regional expression patterns for immunolabelling of the neuropeptide SP, the presynaptic active zone scaffold protein bassoon, and GluA1$^+$-AMPA-Rs in tissue taken from saline-treated mice were consistent with the published literature (**Fig. 2**). Substance P (SP) immunolabelling was restricted to a discrete, dense band across laminae I-IIo of the SCDH (**Fig. 2A**), corresponding to the known innervation zone of peptidergic nociceptive primary afferent fibres. Bassoon (**Fig. 2B**) and GluA1 immunolabelling (**Fig. 2C**) were densely accumulated in the superficial laminae, and present throughout the dorsal horn (see **Fig. 2D** for composite image).

Higher magnification (100×) images reveal that SP immunolabelling forms a dense web of axonal labelling, with many discrete terminal-like structures in the superficial SCDH (**Fig. 2E**). Punctate bassoon (**Fig. 2F**) and GluA1 (**Fig. 2G**) immunolabelling were frequently found in close apposition (**Fig. 2H**, white circles), consistent with presynaptic and postsynaptic proteins, respectively. Most SP$^+$ structures were associated with one or more bassoon puncta (visible as white regions), suggesting the presence of multiple synaptic release sites. Although a few bassoon puncta were associated with GluA1 puncta (white arrowheads), the majority were not. Surprisingly, confocal microscopy did not detect any differences in expression of any of these markers between sections from saline- (**Fig. 3A**) and carrageenan-treated mice (**Fig. 3B**). Quantification of total SCDH GluA1 intensity (**Figs. 3C–E**, 5854 ± 4088 vs 6904 ± 6494, $P = 0.34$) showed no significant increase 24 hours after carrageenan administration. This remained true for all markers even after restoration of confocal images through deconvolution (Supplementary Figs. S3 and 4, available at http://links.lww.com/PAIN/A857), suggesting that any alterations in GluA1 expression occur at the nanoscale, below the detection of diffraction-limited imaging techniques.

3.3. Direct stochastic optical reconstruction microscopy imaging reveals a significant inflammation-induced increase in spinal GluA1 labelling, particularly associated with spinal peptidergic nociceptive terminals

To explore the potential of super-resolution imaging to detect nanoscale alterations in protein expression, we applied dSTORM to the same superficial SCDH field of views used for confocal

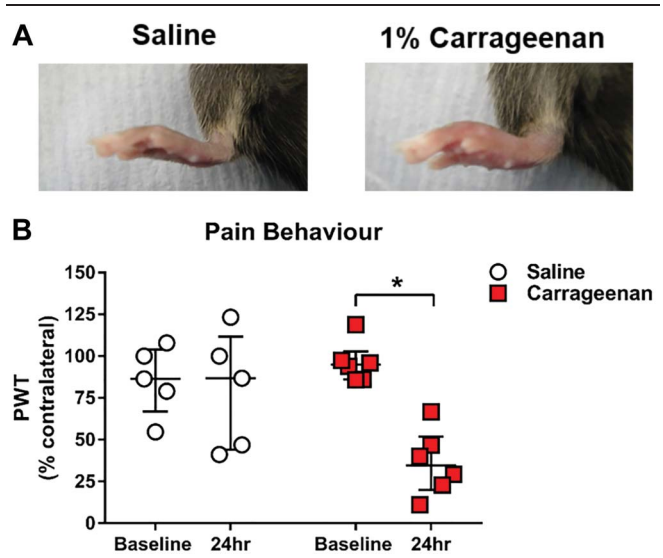

Figure 1. The carrageenan model of subacute inflammatory pain. (A) Representative images of the right hind paw of adult male C57BL/6J mice 24 hours after unilateral intraplantar injection of 10 μL sterile (n = 5) or 1% carrageenan solution (n = 6). One saline-treated animal was excluded due to a misplaced injection. (B) Quantification of 50% ipsilateral PWTs at baseline and 24 hours after injection. Data are expressed as percentage of the contralateral PWT at each time point. Lines = median, error bars = IQR. Within-group changes in PWT over time were assessed using one-tailed Wilcoxon matched-pairs signed rank tests, *$P = 0.0156$. IQR, interquartile range; PWT, paw withdrawal threshold.

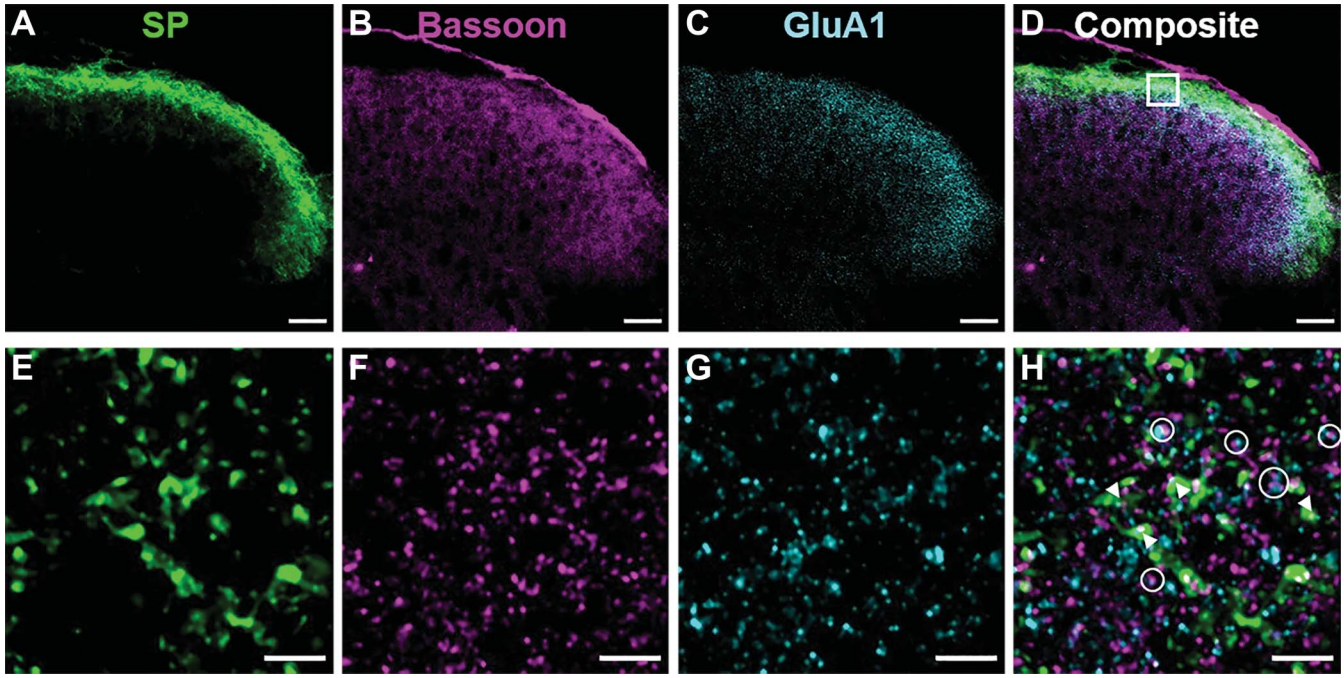

Figure 2. Triple immunolabelling of Substance P (SP), Bassoon, and GluA1 in the spinal cord dorsal horn (SCDH). Representative 20× confocal images of (A) SP, (B) bassoon, and (C) GluA1$^+$-AMPA-R immunolabelling in the SCDH of a saline-treated mouse. A merged image of all 3 channels can be seen in (D). Scale bars = 50 μm. High-magnification (100×) single-channel images showing immunolabelling for (E) SP, (F) bassoon, and (G) GluA1$^+$-AMPA-R taken from the boxed region in (D). (H) Merged image showing an overlay of all 3 channels. White circles highlight close appositions of bassoon and GluA1, and white arrowheads indicate SP$^+$ structures containing bassoon–GluA1 appositions. Scale bars = 5 μm.

analyses. Unlike confocal imaging, dSTORM identified a substantially larger number of individual GluA1 localizations in carrageenan-treated mice (**Fig. 3F–H**; 59% increase, carrageenan = 134,731 ± 28,566, saline = 84,926 ± 50,411, P = 0.0143). This direct comparison between dSTORM and confocal reveals the importance of analysing anatomical correlates of synaptic physiology with nanoscale resolution.

The central terminals of SP-expressing peptidergic nociceptive primary afferent fibres have been identified as the preferential site for functional GluA1-AMPA-R expression in the rodent superficial SCDH.[14,28] We therefore set out to determine how GluA1 expression associated with spinal SP$^+$ structures is altered in the presence of subacute inflammatory pain. Individual SP$^+$ structures containing at least one bassoon punctum (indicative of the presence of a synapse) were selected as ROIs in confocal images using vividSTORM (**Fig. 4**; saline: 191 SP$^+$/bassoon$^+$ ROIs; carrageenan: 231 ROIs). To determine the impact of the inflammatory pain model on the properties of these terminals, the number, size, and labelling intensity of each ROI were quantified. There was a trend towards increased number (**Fig. 5A** carrageenan = 11 ± 5, saline = 8 ± 2, P = 0.0571) and area (**Fig. 5B**; carrageenan = 2.3 ± 0.7, saline = 1.8 ± 0.5 μm^2, P = 0.0571) of SP$^+$/bassoon$^+$ structures in the SCDH of carrageenan-injected mice, suggesting a possible increase in the size and density of peptidergic nociceptive primary afferent terminals induced by the inflammatory pain state. Thus, all subsequent data were normalised to ROI area. There were no significant differences in the average number of bassoon puncta associated within each SP$^+$ ROI (**Fig. 5C**; carrageenan = 1.3 ± 0.5, saline = 1.5 ± 0.3/μm^2, P = 0.49), suggesting no change in the number of synapses formed by each terminal. However, the total number of GluA1 dSTORM localisations associated with SP$^+$ ROIs was almost 10-fold higher in the carrageenan-injected group (**Fig. 5D**; carrageenan = 2560 ± 2004, saline = 272 ± 105, P = 0.0143). Correlation analysis revealed that the number of SP-associated GluA1 localisation points varied inversely with the change in ipsilateral PWTs in the carrageenan-treated group, although this did not reach significance (**Fig. 5E**; r = −0.8, P = 0.1667).

3.4. Targeted analysis of SP$^+$ terminals reveal increased number, but not size, of GluA1$^+$ nanodomains and an increase in the synapse-associated population

GluA2-containing AMPA-Rs at excitatory synapses in hippocampus are arranged in 70 to 80 μm nanodomains.[30,33] To determine whether GluA1$^+$-AMPA-Rs in peptidergic nociceptive primary afferent terminals are similarly organised, Bayesian cluster analysis was performed on GluA1 LPs associated with SP$^+$/bassoon$^+$ ROIs. This analysis identified numerous ~130 nm clusters of GluA1 localisation points, with a significantly larger number of these GluA1 nanodomains associated with SP$^+$ structures in carrageenan-injected mice (**Fig. 5F**; carrageenan = 2.8 ± 0.7 saline = 1.8 ± 0.7, P = 0.0143). Interestingly, neither the median number of LPs per cluster (**Fig. 6A**; carrageenan = 98 ± 10, saline = 91 ± 16, P = 0.1714) nor the diameter of individual GluA1 dSTORM clusters (**Fig. 6B**; carrageenan = 140 ± 11 nm, saline = 127 ± 27 nm, P = 0.1714) was altered in the model of inflammatory pain. Plotting the cumulative frequency analysis of these data confirmed virtually identical size distributions (**Figs. 6C and D**).

To ascertain the potential functional significance of our data, we then asked whether the increase in GluA1 clusters was biased towards association with bassoon immunolabelling, and therefore synaptic release sites. This analysis demonstrated a small 14% increase in non–bassoon-associated extrasynaptic GluA1 clusters in carrageenan-treated mice (**Fig. 6E**, P = 0.1714), but a far larger 34% increase in the number of GluA1 clusters overlapping with, or

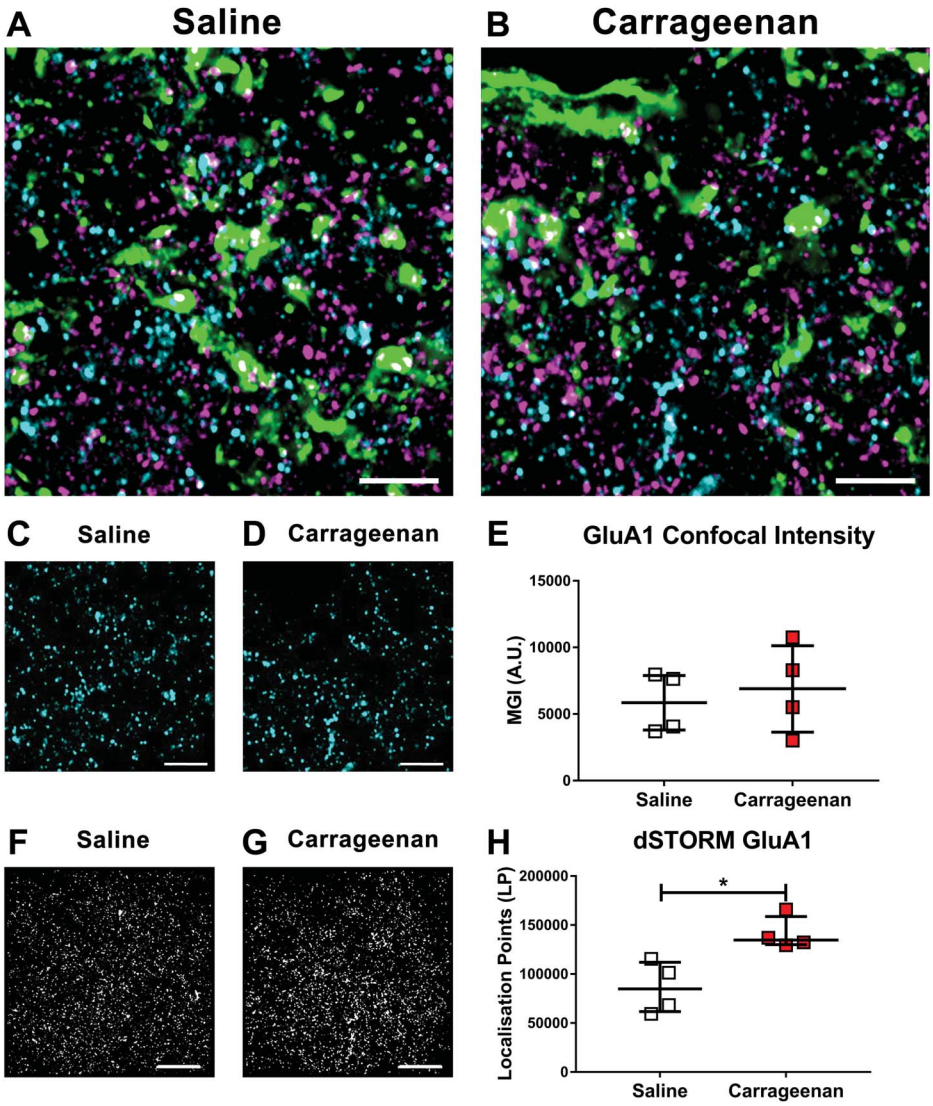

Figure 3. Direct stochastic optical reconstruction microscopy (dSTORM) imaging reveals a significant inflammation-induced increase in spinal GluA1 labelling not detected by confocal microscopy. Representative 100× images of Substance P, bassoon, and GluA1 immunolabelling in the medial superficial spinal cord dorsal horn 24 hours after saline (A) or 1% carrageenan treatment (B). Single-channel confocal (C and D) and unfiltered dSTORM (F and G) images of GluA1 immunolabelling in the same fields of view shown in (A and B). STORM images include all localisations detected from 5000 imaging cycles (see Methods for details). Scale bars = 5 μm. Quantification of confocal mean gray intensity values (E) or total number of STORM localisation points (H) for whole FOV 100× GluA1 immunolabelling. Data are mean values from 3 to 5 field of view per animal, 4 animals per group. Line = median, error bars = IQR. *P = 0.0143, one-tailed Mann–Whitney U test.

directly apposed to, bassoon (**Fig. 6F**; carrageenan = 1.2 ± 0.4 vs saline = 0.9 ± 0.4, P = 0.0286). Comparison of the frequency distributions reveals little change in non–synapse-associated GluA1 (**Fig. 6G**) but that the number of bassoon puncta without detectable GluA1 was almost halved 24 hours after induction of the carrageenan model (**Fig. 6H**; carrageenan = 15.85%, saline = 31.25%). This analysis also identified a small population of ROIs with a very high number of bassoon-associated GluA1 clusters (>6) in the sections from the carrageenan model.

4. Discussion

To the best of our knowledge, this is the first study to apply STORM super-resolution imaging to probe the anatomical correlates of pain. Super-resolution microscopy can precisely determine the nanoscale distributions of target molecules[1,11,46] and reveal previously inaccessible subdiffraction limit structural motifs.[16,40,50] Herein, the exquisite sensitivity of dSTORM revealed that behavioral hypersensitivity in the mouse carrageenan model of subacute inflammatory pain is accompanied by increased expression of calcium-permeable GluA1$^+$-AMPA-Rs in the SCDH. Cell type–specific analyses identified a substantial contribution of GluA1 associated with SP$^+$ structures, the majority of which are central terminals of peptidergic nociceptive primary afferent fibers.[25,41] As the number of individual GluA1 nanodomains scaled with the extent of hypersensitivity, we suggest increased unitary addition of GluA1 nanodomains as a potential anatomical correlate of inflammatory pain.

4.1. Increased spinal GluA1 expression at spinal peptidergic nociceptive terminals

Peripheral injection of carrageenan produces biphasic inflammation, with a rapidly developing initial component resolving within 6

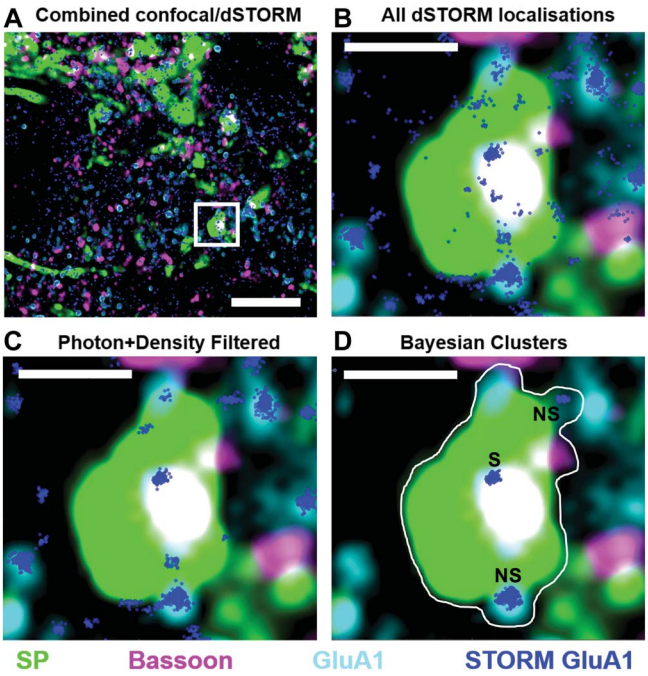

Figure 4. Targeted cell type–specific analyses of SP$^+$ structures. (A) Overlay of 3-channel confocal image and GluA1 STORM localisation points (dark blue) taken from a representative section in a saline-treated mouse. (B–D) An enlargement of the boxed region in (A), showing a SP$^+$ structure with 2 associated bassoon puncta (magenta/white) and all GluA1 STORM localisation points (B), and the same structure after density and photon filtering of STORM localisations (C), and after manual selection of the ROI and Bayesian cluster analysis to isolate individual GluA1 clusters (D). Each cluster was designated as synapse-associated (S) or non–synapse-associated (NS) based on visual analyses of overlap with or proximity to bassoon labelling.

hours, and a more pronounced late phase peaking at 24 to 48 hours and persisting for up to 4 days.[22,36] The latter subacute phase was studied here because it is associated with plasticity in spinal nociceptive circuitry, and altered ion channel expression in primary afferent fibres.[29]

Substantial upregulation of GluA1, but not GluA2, has been previously been demonstrated in isolated lumbar spinal cord membrane fractions in the carrageenan model through Western blotting.[48] However, subsequent immunohistochemical analyses detected no change in total GluA1 in the superficial SCDH. Similarly, we report that confocal microscopy was unable to detect an alteration in total GluA1 immunolabelling in the superficial SCDH 24 hours after carrageenan, even after image restoration through deconvolution. By contrast, dSTORM analyses of the same immunolabelling identified a 59% increase in GluA1, demonstrating the enhanced sensitivity of STORM compared with diffraction-limited imaging techniques. Virtually, all AMPA-Rs in the superficial laminae of the rodent spinal cord, including all GluA1$^+$ receptors, contain GluA2[35]; therefore, increased GluA1 expression either represents replacement of GluA1-negative AMPA-Rs with heteromers containing both GluA1 and GluA2, or insertion of additional GluA1$^+$ receptors. This increase in GluA1 immunolabelling was significant despite variability in expression levels between animals, and relatively small group sizes, and therefore dSTORM imaging also has the potential to reduce the numbers of animals required in future anatomical studies.

Alongside increased resolution, another major advantage of STORM is its compatibility with multiplex fluorescent immunolabelling. This enables large-scale quantitative cell type–specific analyses that are extremely laborious and expensive to perform through electron microscopy. We took advantage of this to focus our investigations on SP$^+$ structures containing at least one synapse, the majority of which are the central terminals of peptidergic nociceptive primary afferents,[25,41] where GluA1 subunits are preferentially expressed.[14,28] It is important to note, however, that a population of intrinsic spinal neurons also express SP[17] and have some axons projecting to lamina I,[19] and are involved in nociceptive signalling. It is possible that some terminals arising from these cells form a portion of the structures analysed here. For clarity, we have therefore used the terminology of spinal peptidergic nociceptive terminals throughout. In structures immunoreactive for the neuropeptide SP and the presynaptic active zone marker bassoon (and thus the presumed presence of a nociceptive peptidergic synapse), we report 10-fold higher levels of GluA1 in carrageenan-treated mice compared with saline-treated controls. The higher levels of GluA1 expression in SP$^+$ structures were associated with lower mechanical pain thresholds in carrageenan-treated mice, but not in saline-treated mice, although this association did not reach statistical significance. These data suggest that GluA1 expression at spinal peptidergic nociceptive terminals is unrelated to basal mechanical pain sensitivity, but scales with behavioural hypersensitivity after an inflammatory insult, further supporting a functional link between calcium-permeable AMPA-R expression, synaptic plasticity, and pain behavior in this model of inflammatory pain.

4.2. Increased numbers of individual GluA1$^+$-AMPA-R nanodomains at spinal peptidergic nociceptive terminals

Recent work identified the role of transsynaptically aligned nanodomains in the regulation of neurotransmission,[4] and super-resolution imaging has been used to demonstrate nanoscale clustering of glutamate receptors in 70 to 80 nm domains at hippocampal excitatory synapses.[30,33] Here, we used Bayesian cluster analysis to identify individual GluA1 nanodomains associated with spinal peptidergic nociceptive terminals. We report the presence of numerous discrete ~130 nm GluA1 nanodomains, and demonstrate a 54% increase in their number in carrageenan- vs saline-treated mice, with no significant change in their size or density. These nanodomains are larger than those previously described for GluA2,[30,33] which may be accounted for by the larger size of central primary afferent fiber terminals compared with hippocampal synapses. The presence of a small population of terminals with a very high number of GluA1 clusters raises the intriguing possibility that synaptic plasticity in just a few individual terminals could have a significant contribution to altered nociceptive signaling in inflammatory pain states. Importantly, the increase in average number, but not size, of GluA1 nanodomains is concordant with reports in hippocampal spines,[23] where synaptic strength scales with synapse size through coordinated addition of unitary synaptic modules, rather than increase in individual unit size. Our data indicate that similar principles may govern the organization of spinal GluA1, and point to a functional alteration in glutamate sensitivity at spinal peptidergic nociceptive terminals as an anatomical correlate of subacute inflammatory pain.

4.3. Increased GluA1 clusters at synaptic release sites of spinal peptidergic nociceptive terminals

Previous investigations in inflammatory pain models failed to show a change in total spinal GluA1 expression through

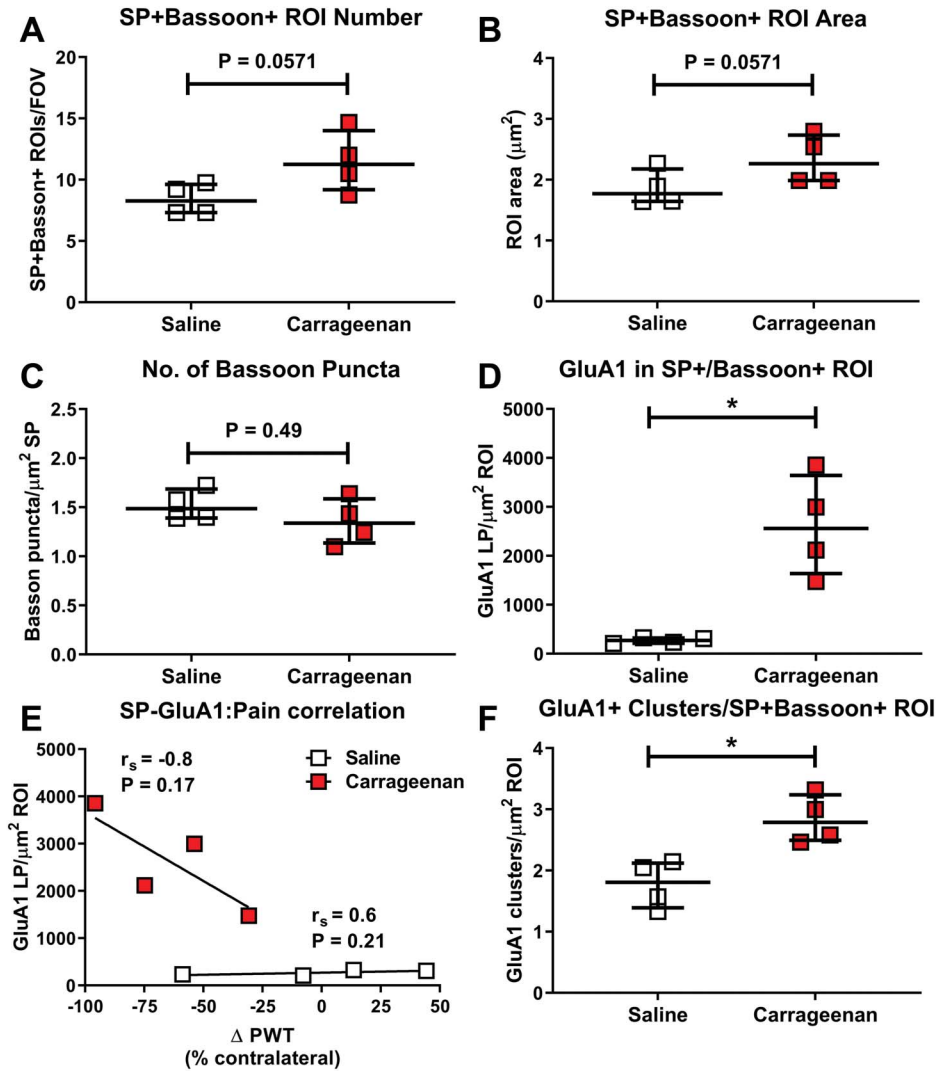

Figure 5. Targeted dSTORM analyses reveal increased GluA1 at spinal SP^+ nociceptive terminals. Quantification of $SP^+Bassoon^+$ ROIs reveals a trend towards increased average number per FOV (A), and individual ROI area (B), but no change in the number of bassoon puncta associated with each ROI (C) in carrageenan-treated mice (median ± interquartile range). Quantification of carrageenan-induced changes in GluA1 clusters associated with $SP^+Bassoon^+$ ROIs (all data normalised to ROI area in μm^2, line = median, error bars = interquartile range) demonstrates a significant increase in the average total number of GluA1 LPs associated with individual SP^+ ROIs in carrageenan-treated mice (D). The average number of GluA1 localisations correlates with pain behaviour in individual carrageenan-treated, but not saline-treated, mice (E). Pain behaviour is expressed as % change in normalised ipsilateral PWTs, and correlations assessed using Spearman's *r*. The average number of GluA1 clusters associated with SP^+ ROIs is also increased in carrageenan- vs saline-treated mice, normalised to ROI area (F). Individual clusters were identified through Bayesian cluster analysis for each $SP^+Bassoon^+$ ROI. $^*P < 0.05$, Mann–Whitney *U* test. dSTORM, direct stochastic optical reconstruction microscopy; FOV, field of view; LP, localisation point; PWT, paw withdrawal threshold; ROI, region of interest.

diffraction-limited light microscopy, but indicated a shift in the proportion of GluA1 immunolabelling associated with the synaptic marker synaptophysin.[48] Physiological data from the complete Freund's adjuvant model has also identified a switch to calcium-mediated signalling at synapses expressing the receptor for SP, NK1-R.[47] Taken together, these observations suggest that specific synaptic insertion of GluA1 may be a key feature of synaptic plasticity in subacute inflammatory pain.

To interrogate synapse-specific changes in our data set, we determined whether GluA1 clusters in SP^+ structures were preferentially associated with the presynaptic active zone marker bassoon, and thus the presumed position of a synapse. A slight increase in extrasynaptic (non–bassoon-associated) GluA1 clusters was observed, which may contribute to altered synaptic physiology through detection of volume transmission or synaptic overflow of glutamate. However, the largest difference was in synapse-associated GluA1. The average number of GluA1 clusters associated with each SP^+ synapse was significantly higher in carrageenan-treated mice when compared with saline-treated controls, and the population of SP^+ synapses without detectable GluA1 immunoreactivity was halved. These data further support the specific synaptic insertion of calcium-permeable AMPA-R subunits at spinal peptidergic nociceptive terminals in the model of inflammatory hyperalgesia.

4.4. Study limitations

We note several caveats relating to the study design and some inherent technical limitations of the approach. As with all immunohistochemical approaches, dSTORM is reliant on the affinity and specificity of the antibodies (see Supplementary Materials, available at http://links.lww.com/PAIN/A857). It should

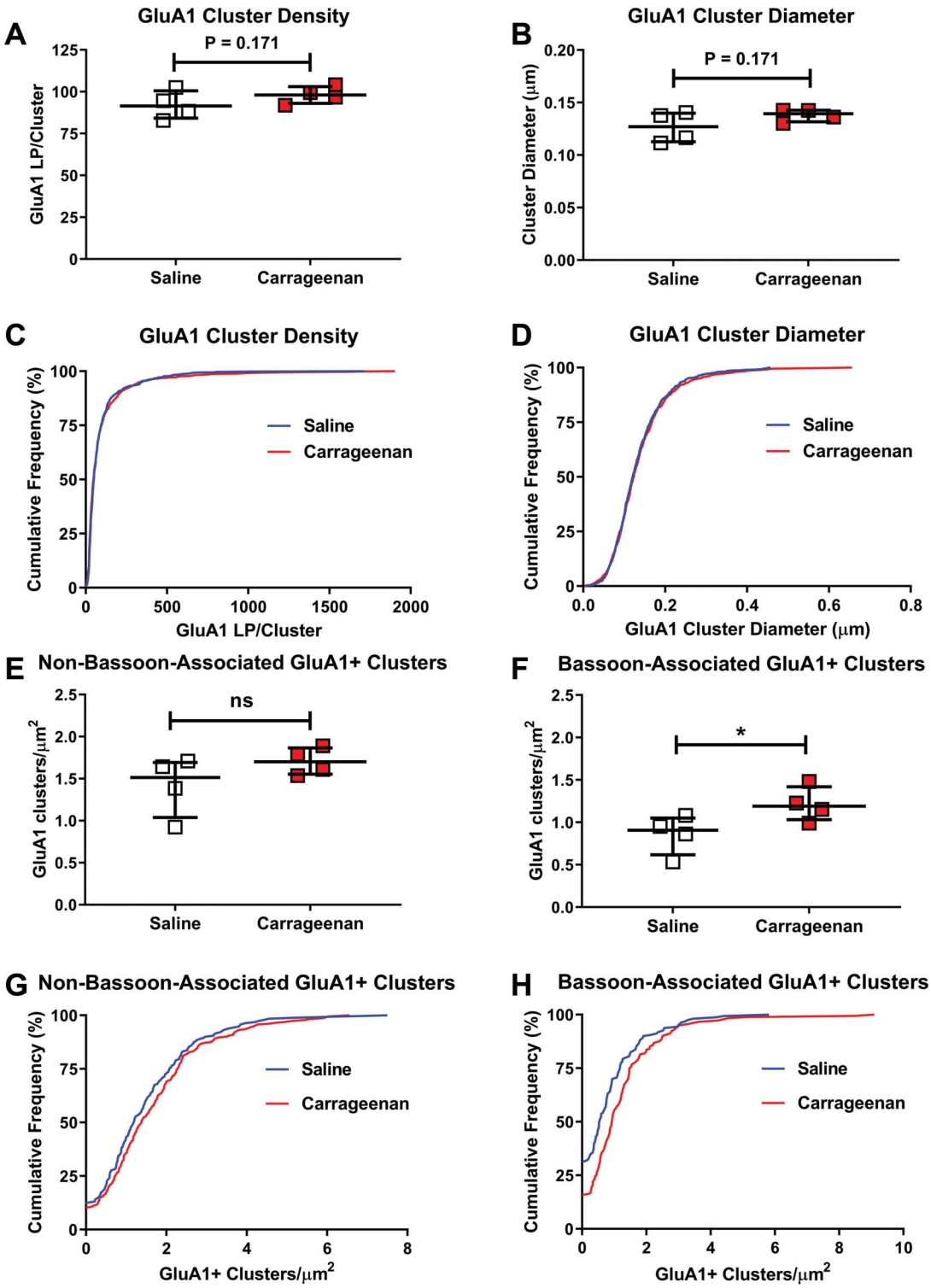

Figure 6. Increased number, but not size or density, of GluA1$^+$ nanodomains associated with spinal SP$^+$ nociceptive terminals as an anatomical correlate of inflammatory pain. Quantification of the average number of GluA1 dSTORM localisations within each individual nanodomain (A), and the average diameter of GluA1 nanodomains (B) show no significant changes 24 hours after carrageenan. The corresponding cumulative frequency distributions (C and D) reveal largely overlapping populations, except for the presence of a small number of very large nanodomains (diameter >0.5 μm) in the carrageenan-treated group. Individual analyses of identified GluA1 nanodomains revealed a small, nonsignificant increase in the non–bassoon-associated population (E) but a larger increase in GluA1 associated with bassoon puncta (F). Cumulative frequency analyses reveal largely overlapping distributions of non–bassoon-associated GluA1 (G), but a rightward shift in the number of GluA1 nanodomains associated with bassoon puncta (H). Individual data points represent mean values for individual animals, lines = group median values, error bars = interquartile range. *$P < 0.05$, one-tailed Mann–Whitney U tests. LP, localisation point; dSTORM, direct stochastic optical reconstruction microscopy.

be noted that localisation precision is limited by the size of the antibody complex (~7-8nm per IgG[45]), and the pixel size of the detectors, rather than the theoretical limit of the size of fluorophore (~1 nm). Despite the increased sensitivity of STORM compared with diffraction-limited imaging approaches, there is still a limit of detection, and a lack of labelling should not be interpreted as total absence of protein; thus, our numerical findings are not absolute, eg, the proportion of structures containing GluA1. The synaptic markers in this study were imaged through less sensitive confocal microscopy, and some weakly immunoreactive structures may therefore have been missed, leading to some synaptic GluA1 clusters being incorrectly attributed. However, we note that the proportion of synapses lacking GluA1 in saline-treated animals detected herein (31.25%) closely approximates that reported for the whole superficial dorsal horn (~35%).[35] Future studies using multichannel dSTORM will enable more precise determination of the relationship between key synaptic components, and how this nanoscale organization contributes to plasticity.

Direct stochastic optical reconstruction microscopy cannot be considered truly quantitative due to the nonlinear relationship between antigen, primary antibody, secondary antibody, and fluorophore, and the probability of individual fluorophores undergoing multiple photoswitching cycles. Thus, whether LPs in close proximity indicate the presence of multiple GluA1$^+$-AMPA-Rs, a single AMPA-R multiply labelled with primary and/or secondary antibodies, or a single receptor-antibody complex in which the fluorophore underwent multiple photoswitching cycles cannot be distinguished. However, these considerations are applicable across all experimental conditions, and therefore the ratiometric comparisons used here are robust and are unlikely to impact on effect size.

A final consideration is that pools of AMPA-Rs are not static, but highly dynamic,[7] with changes in their mobility underpinning aspects of synaptic plasticity. Our use of fixed tissue in this study provides only a single snapshot of GluA1 localisation, and thus future studies using single-molecule tracking super-resolution imaging techniques such as uPAINT or sptPALM will be required to determine the time course and dynamics of inflammation-induced alterations in spinal GluA1 expression.

5. Conclusion

In the carrageenan model, inflammatory pain was accompanied by increased expression of calcium-permeable GluA1$^+$-AMPA-Rs in the SCDH. A substantial proportion of GluA1$^+$-AMPA-Rs were associated with spinal peptidergic nociceptive terminals and the number of individual GluA1$^+$ nanodomains at these terminals scaled with behavioral hypersensitivity. Many more GluA1 nanodomains were associated with the presynaptic active zone marker bassoon, supporting synaptic insertion of calcium-permeable AMPA-R subunits at spinal peptidergic nociceptive terminals as a functional marker in this model of inflammatory hyperalgesia.

Conflict of interest statement

The authors have no conflicts of interest to declare.

Acknowledgements

The authors thank Judit Glavincs, Vivien Miczan, and Istvan Katona from the Institute of Experimental Medicine in Budapest for useful discussions relating to STORM image analysis through vividSTORM, and Seema Bagia for technical assistance with deconvolution of confocal images.
Super-resolution microscopy was performed at the School of Life Sciences Imaging (SLIM) facility, University of Nottingham.
This work was supported by an internal grant from the University of Nottingham; Arthritis Research United Kingdom (grants 18769, 20777); and the Zeiss Elyra PS1 super resolution microscope was funded by a BBSRC grant (BB/L013827/1—Multidisciplinary Super Resolution Microscopy Facility).
Author contributions: All authors were involved in drafting the article or revising it for important intellectual content, and approved the final version. Study concept and design: S.G. Woodhams, R. Markus, P.R.W. Gowler, T.G. Self, and V. Chapman. Data acquisition: S.G. Woodhams, P.R.W. Gowler, and R. Markus. Data analysis: S.G. Woodhams. Manuscript: S.G. Woodhams, R. Markus, P.R.W. Gowler, T.G. Self, and V. Chapman.

Appendix A. Supplemental digital content

Supplemental digital content associated with this article can be found online at http://links.lww.com/PAIN/A857.

Article history:
Received 11 May 2019
Received in revised form 15 July 2019
Accepted 30 July 2019
Available online 15 August 2019

References

[1] Baddeley D, Jayasinghe ID, Lam L, Rossberger S, Cannell MB, Soeller C. Optical single-channel resolution imaging of the ryanodine receptor distribution in rat cardiac myocytes. Proc Natl Acad Sci U S A 2009;106:22275–80.
[2] Barna L, Dudok B, Miczan V, Horvath A, Laszlo ZI, Katona I. Correlated confocal and super-resolution imaging by VividSTORM. Nat Protoc 2016;11:163–83.
[3] Beazley-Long N, Moss CE, Ashby WR, Bestall SM, Almahasneh F, Durrant AM, Benest AV, Blackley Z, Ballmer-Hofer K, Hirashima M, Hulse RP, Bates DO, Donaldson LF. VEGFR2 promotes central endothelial activation and the spread of pain in inflammatory arthritis. Brain Behav Immun 2018;74:49–67.
[4] Biederer T, Kaeser PS, Blanpied TA. Transcellular nanoalignment of synaptic function. Neuron 2017;96:680–96.
[5] Binder DA. Bayesian cluster analysis. Biometrika 1978;65:31–8.
[6] Boyle KA, Gutierrez-Mecinas M, Polgár E, Mooney N, O'Connor E, Furuta T, Watanabe M, Todd AJ. A quantitative study of neurochemically defined populations of inhibitory interneurons in the superficial dorsal horn of the mouse spinal cord. Neuroscience 2017;363:120–33.
[7] Choquet D. Linking nanoscale dynamics of AMPA receptor organization to plasticity of excitatory synapses and learning. J Neurosci 2018;38:9318–29.
[8] De Pace R, Skirzewski M, Damme M, Mattera R, Mercurio J, Foster AM, Cuitino L, Jarnik M, Hoffmann V, Morris HD, Han TU, Mancini GMS, Buonanno A, Bonifacino JS. Altered distribution of ATG9A and accumulation of axonal aggregates in neurons from a mouse model of AP-4 deficiency syndrome. PLoS Genet 2018;14:e1007363.
[9] Dick O, tom Dieck S, Altrock WD, Ammermüller J, Weiler R, Garner CC, Gundelfinger ED, Brandstätter JH. The presynaptic active zone protein bassoon is essential for photoreceptor ribbon synapse formation in the retina. Neuron 2003;37:775–86.
[10] Duan B, Cheng L, Bourane S, Britz O, Padilla C, Garcia-Campmany L, Krashes M, Knowlton W, Velasquez T, Ren X, Ross Sarah E, Lowell Bradford B, Wang Y, Goulding M, Ma Q. Identification of spinal circuits transmitting and gating mechanical pain. Cell 2014;159:1417–32.
[11] Ehmann N, van de Linde S, Alon A, Ljaschenko D, Keung XZ, Holm T, Rings A, DiAntonio A, Hallermann S, Ashery U, Heckmann M, Sauer M, Kittel RJ. Quantitative super-resolution imaging of Bruchpilot distinguishes active zone states. Nat Commun 2014;5:4650.

[12] Engelman HS, Allen TB, MacDermott AB. The distribution of neurons expressing calcium-permeable AMPA receptors in the superficial laminae of the spinal cord dorsal horn. J Neurosci 1999;19:2081–9.
[13] François A, Low SA, Sypek EI, Christensen AJ, Sotoudeh C, Beier KT, Ramakrishnan C, Ritola KD, Sharif-Naeini R, Deisseroth K, Delp SL, Malenka RC, Luo L, Hantman AW, Scherrer G. A brainstem-spinal cord inhibitory circuit for mechanical pain modulation by GABA and enkephalins. Neuron 2017;93:822–39.e826.
[14] Gangadharan V, Wang R, Ulzhöfer B, Luo C, Bardoni R, Bali KK, Agarwal N, Tegeder I, Hildebrandt U, Nagy GG, Todd AJ, Ghirri A, Häussler A, Sprengel R, Seeburg PH, MacDermott AB, Lewin GR, Kuner R. Peripheral calcium-permeable AMPA receptors regulate chronic inflammatory pain in mice. J Clin Invest 2011;121:1608–23.
[15] Greenspon CM, Battell EE, Devonshire IM, Donaldson LF, Chapman V, Hathway GJ. Lamina-specific population encoding of cutaneous signals in the spinal dorsal horn using multi-electrode arrays. J Physiol 2019;597:377–97.
[16] Grosse L, Wurm CA, Bruser C, Neumann D, Jans DC, Jakobs S. Bax assembles into large ring-like structures remodeling the mitochondrial outer membrane in apoptosis. EMBO J 2016;35:402–13.
[17] Gutierrez-Mecinas M, Bell AM, Marin A, Taylor R, Boyle KA, Furuta T, Watanabe M, Polgár E, Todd AJ. Preprotachykinin A is expressed by a distinct population of excitatory neurons in the mouse superficial spinal dorsal horn including cells that respond to noxious and pruritic stimuli. PAIN 2017;158:440–56.
[18] Gutierrez-Mecinas M, Furuta T, Watanabe M, Todd AJ. A quantitative study of neurochemically defined excitatory interneuron populations in laminae I–III of the mouse spinal cord. Mol Pain 2016;12:1–18.
[19] Gutierrez-Mecinas M, Polgár E, Bell AM, Herau M, Todd AJ. Substance P-expressing excitatory interneurons in the mouse superficial dorsal horn provide a propriospinal input to the lateral spinal nucleus. Brain Struct Funct 2018;223:2377–92.
[20] Hachisuka J, Baumbauer KM, Omori Y, Snyder LM, Koerber HR, Ross SE. Semi-intact ex vivo approach to investigate spinal somatosensory circuits. eLife 2016;5:e22866.
[21] Häring M, Zeisel A, Hochgerner H, Rinwa P, Jakobsson JET, Lönnerberg P, La Manno G, Sharma N, Borgius L, Kiehn O, Lagerström MC, Linnarsson S, Ernfors P. Neuronal atlas of the dorsal horn defines its architecture and links sensory input to transcriptional cell types. Nat Neurosci 2018;21:869–80.
[22] Henriques MG, Silva PM, Martins MA, Flores CA, Cunha FQ, Assreuy-Filho J, Cordeiro RS. Mouse paw edema. A new model for inflammation? Braz J Med Biol Res 1987;20:243–9.
[23] Hruska M, Henderson N, Le Marchand SJ, Jafri H, Dalva MB. Synaptic nanomodules underlie the organization and plasticity of spine synapses. Nat Neurosci 2018;21:671–82.
[24] Huang B, Bates M, Zhuang X. Super resolution fluorescence microscopy. Annu Rev Biochem 2009;78:993–1016.
[25] Jessell T, Tsunoo A, Kanazawa I, Otsuka M. Substance P depletion in the dorsal horn of rat spinal cord after section of the peripheral processes of primary sensory neurons. Brain Res 1979;168:247–59.
[26] Kilkenny C, Browne WJ, Cuthill IC, Emerson M, Altman DG. Improving bioscience research reporting: the ARRIVE guidelines for reporting animal research. PLoS Biol 2010;8:e1000412.
[27] Koch SC, Acton D, Goulding M. Spinal circuits for touch, pain, and itch. Annu Rev Physiol 2018;80:189–217.
[28] Lee CJ, Bardoni R, Tong CK, Engelman HS, Joseph DJ, Magherini PC, MacDermott AB. Functional expression of AMPA receptors on central terminals of rat dorsal root ganglion neurons and presynaptic inhibition of glutamate release. Neuron 2002;35:135–46.
[29] Lolignier S, Amsalem M, Maingret F, Padilla F, Gabriac M, Chapuy E, Eschalier A, Delmas P, Busserolles J. Nav1.9 channel contributes to mechanical and heat pain hypersensitivity induced by subacute and chronic inflammation. PLoS One 2011;6:e23083.
[30] MacGillavry Harold D, Song Y, Raghavachari S, Blanpied Thomas A. Nanoscale scaffolding domains within the postsynaptic density concentrate synaptic AMPA receptors. Neuron 2013;78:615–22.
[31] McLeod AL, Krause JE, Ribeiro-da-Silva A. Immunocytochemical localization of neurokinin B in the rat spinal dorsal horn and its association with substance P and GABA: an electron microscopic study. J Comp Neurol 2000;420:349–62.
[32] Nägerl UV, Sibarita JB. Special section guest editorial: super-resolution microscopy of neural structure and function. Neurophotonics 2016;3:041801.
[33] Nair D, Hosy E, Petersen JD, Constals A, Giannone G, Choquet D, Sibarita JB. Super-resolution imaging reveals that AMPA receptors inside synapses are dynamically organized in nanodomains regulated by PSD95. J Neurosci 2013;33:13204–24.
[34] Polgar E, Furuta T, Kaneko T, Todd A. Characterization of neurons that express preprotachykinin B in the dorsal horn of the rat spinal cord. Neuroscience 2006;139:687–97.
[35] Polgar E, Watanabe M, Hartmann B, Grant SG, Todd AJ. Expression of AMPA receptor subunits at synapses in laminae I-III of the rodent spinal dorsal horn. Mol Pain 2008;4:5.
[36] Posadas I, Bucci M, Roviezzo F, Rossi A, Parente L, Sautebin L, Cirino G. Carrageenan-induced mouse paw oedema is biphasic, age-weight dependent and displays differential nitric oxide cyclooxygenase-2 expression. Br J Pharmacol 2004;142:331–8.
[37] Rexed B. The cytoarchitectonic organization of the spinal cord in the cat. J Comp Neurol 1952;96:415–95.
[38] Rust MJ, Bates M, Zhuang X. Sub-diffraction-limit imaging by stochastic optical reconstruction microscopy (STORM). Nat Methods 2006;3:793.
[39] Shi SH, Hayashi Y, Petralia RS, Zaman SH, Wenthold RJ, Svoboda K, Malinow R. Rapid spine delivery and redistribution of AMPA receptors after synaptic NMDA receptor activation. Science 1999;284:1811–16.
[40] Sigal YM, Zhou R, Zhuang X. Visualizing and discovering cellular structures with super-resolution microscopy. Science 2018;361:880–7.
[41] Taquet H, Plachot JJ, Pohl M, Collin E, Benoliel JJ, Bourgoin S, Mauborgne A, Meunier JC, Cesselin F, Hamon M. Increased calcitonin gene-related peptide- and cholecystokinin-like immunoreactivities in spinal motoneurones after dorsal rhizotomy. J Neural Transm Gen Sect 1992;88:127–41.
[42] tom Dieck S, Sanmartí-Vila L, Langnaese K, Richter K, Kindler S, Soyke A, Wex H, Smalla KH, Kämpf U, Fränzer JT, Stumm M, Garner CC, Gundelfinger ED. Bassoon, a novel zinc-finger CAG/Glutamine-repeat protein selectively localized at the active zone of presynaptic nerve terminals. J Cell Biol 1998;142:499–509.
[43] Urch CE, Dickenson AH. In vivo single unit extracellular recordings from spinal cord neurones of rats. Brain Res Brain Res Protoc 2003;12:26–34.
[44] Usoskin D, Furlan A, Islam S, Abdo H, Lönnerberg P, Lou D, Hjerling-Leffler J, Haeggström J, Kharchenko O, Kharchenko PV, Linnarsson S, Ernfors P. Unbiased classification of sensory neuron types by large-scale single-cell RNA sequencing. Nat Neurosci 2014;18:145.
[45] van de Linde S, Löschberger A, Klein T, Heidbreder M, Wolter S, Heilemann M, Sauer M. Direct stochastic optical reconstruction microscopy with standard fluorescent probes. Nat Protoc 2011;6:991.
[46] van de Linde S, Sauer M, Heilemann M. Subdiffraction-resolution fluorescence imaging of proteins in the mitochondrial inner membrane with photoswitchable fluorophores. J Struct Biol 2008;164:250–4.
[47] Vikman KS, Rycroft BK, Christie MJ. Switch to Ca2+-permeable AMPA and reduced NR2B NMDA receptor-mediated neurotransmission at dorsal horn nociceptive synapses during inflammatory pain in the rat. J Physiol 2008;586:515–27.
[48] Wigerblad G, Huie JR, Yin HZ, Leinders M, Pritchard RA, Koehrn FJ, Xiao WH, Bennett GJ, Huganir RL, Ferguson AR, Weiss JH, Svensson CI, Sorkin LS. Inflammation-induced GluA1 trafficking and membrane insertion of Ca2+ permeable AMPA receptors in dorsal horn neurons is dependent on spinal tumor necrosis factor, PI3 kinase and protein kinase A. Exp Neurol 2017;293:144–58.
[49] Woolf CJ. Evidence for a central component of post-injury pain hypersensitivity. Nature 1983;306:686–8.
[50] Xu J, Ma H, Jin J, Uttam S, Fu R, Huang Y, Liu Y. Super-resolution imaging of higher-order chromatin structures at different epigenomic states in single mammalian cells. Cell Rep 2018;24:873–82.
[51] Yamanaka M, Smith NI, Fujita K. Introduction to super-resolution microscopy. Microscopy 2014;63:177–92.
[52] Zhuang X. Nano-imaging with STORM. Nat Photon 2009;3:365–7.